Gas-phase hydration of nopinone: the interplay between theoretical methods and experiments unveils the conformational landscape

Elias Neeman, Juan Ramón Avilés Moreno, Thérèse Huet

Gas-phase hydration of nopinone: the interplay between theoretical methods and experiments unveils the conformational landscape

Elias M. Neeman,* Juan Ramón Avilés Moreno‡ and Thérèse R. Huet

The structure of microsolvated nopinone formed in the supersonic jet expansion is investigated in the gas phase. The rotational spectra of nopinone···$(H_2O)_n$ (n=1,2,3) were analysed by means of Fourier transform microwave spectroscopy. In the present study, three monohydrates, two dihydrates as well as two trihydrates were observed and characterized. The observed structures are the lowest energy conformers predicted by quantum chemical calculations. In all the observed hydrates of nopinone, water was found to be linked to the ketone group (C=O) with a strong hydrogen bond (O_{NOP}···H_W) and finishing with a dispersive one (O_W···H_{NOP}). The structure of nopinone was found to alter the structure of water dimer and water trimer, which make nopinone to be surrounding with a chain of water molecules. A remarkable decreasing in the H-bonding length was observed when the number of attached water is increased. Different DFT and *ab initio* calculations at the equilibrium structure allowed the identification of the observed conformers. Evaluation of the B3LYP-D3 and ωB97X-D results revealed deficiencies to reproduce the structure of one observed monohydrated structure while MP2 and M06-2X reproduce all the three observed structures. A comparison with similar bicyclic ketone highlights how a small change in the bicyclic ring leads to different effects in the microsolvatation of Biogenic VOCs. This study presents the first step of molecular aggregation to understand the atmospheric formation of aerosols at the molecular scale.

Introduction

The volatile organic compounds (VOCs) are biogenic and anthropogenic particles suspended in the earth's atmosphere. Their tropospheric oxidations with ozone, nitrogen oxides and hydroxyl radicals contribute to the formation of atmospheric aerosols which represent a major environmental problem. They degrade visibility and affect human health.[1,2] They also directly or indirectly influence the climate by absorbing and reflecting solar radiation, or by modifying cloud formation.[3] The aerosol formation processes are still not well understood.[4,5] The pre-nucleation clusters process is the first step. A molecular complex forms the critical nucleus and then grows to a detectable size.[3,6] Hydrogen-bond interactions are one of the several elements responsible for the formation of atmospheric relevant species.[7] Several experimental studies[8–10] were performed in the laboratory to understand the formation of secondary organic aerosols (SOA) from VOCs and its relation with water. Those studies have shown that SOA formation is enhanced by the water presence.[8–10] Actually, the aerosol formation process is directly related to relative humidity (RH) and the aerosol quantity increases with the increasing of the RH.[8–10] Moreover several chemical reactions in the atmosphere start by the formation of non-covalent complexes. So far H-bonding is one of the most important non-covalent interactions, which plays also a critical role in many biological and chemical processes.[11,12]

This information evidences the relevance of studying H-bonding interactions between water and oxygenated VOCs. High-resolution Fourier transform microwave (FTMW) spectroscopy combined with theoretical calculations is a powerful tool to study complex systems in the gas phase. This combination has allowed the identification of flexible conformational landscape[13–15] and the favourable hydration sites.[16–23] Recently, microsolvated clusters, which present the first step of hydration have been object of experimental[18–23] and theoretical[24,25] studies. Previous studies[19,26] on monoterpenoids have shown the possibility to surround ketone molecules by a chain of three water molecules. For example, in the case of both verbenone ($C_{10}H_{14}O$, 4,6,6-trimethylbicyclo[3.1.1]hept-3-en-2-one) and camphor, ($C_{10}H_{16}O$, 1,7,7-trimethylbicyclo[2.2.1]hepta-2-one) two monohydrates, two dihydrates and one trihydrate have been observed and characterized. In the case of alcohol monoterpenoid, fenchol,[13] only monohydrate cluster was observed.[14] Coming back to bicyclic ketones, it is interesting to evaluate how the change of the bicyclic ketone unit can affect the formation of the hydrated conformational behaviour: would the structure of ketone play an important role in the stabilization of hydrate structures, and how it contributes to the

Univ. Lille, CNRS, UMR 8523 - PhLAM - Physique des Lasers Atomes et Molécules, F-59000 Lille, France.
‡ *Present address: Department of Applied Physical Chemistry, Universidad Autónoma de Madrid, 28049, Madrid, Spain.*
* Corresponding author: elias.neeman@univ-lille.fr, https://orcid.org/0000-0002-6662-7784.
Electronic Supplementary Information (ESI) available: [observed transitions, optimised conformers structures]. See DOI: 10.1039/x0xx00000x

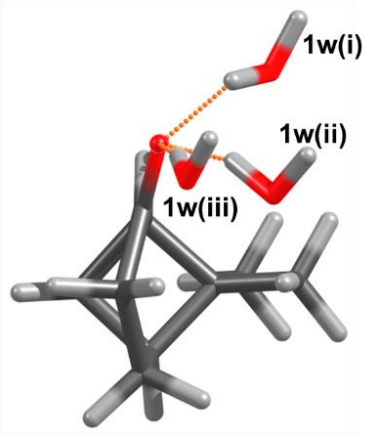

Figure 1. Illustration of the monohydrate clusters, the position of NOP is fixed to help visualization. As it shown the position of water conformers 1w(ii) and 1w(iii) is close. This fact can explain the non-convergence of some DFT methods for those structures.

stabilization of further conformers? With this aim, we report on the analysis of nopinone-water clusters using impulse Fabry-Pérot Fourier-transform microwave spectroscopy technique coupled to a pulsed supersonic jet expansion (FP-FTMW spectrometer). Nopinone ($C_9H_{14}O$, 6,6-dimethylbicyclo[3.1.1]heptan-2-one) represents the major oxidation product of β-pinene ($C_{10}H_{16}$, 6,6-dimethyl-2-methylenebicyclo[3.1.1]heptane) in the atmosphere.[27] In a previous study, we have demonstrated that during the oxidation process the structure of the precursor β-pinene and of the oxidized product Nopinone (labelled as NOP from now on) is maintained in the gas phase.[28] Different theoretical methods were performed in order to guide the identification of the observed hydrates species. This study is relevant to understand the hydration processes at the molecular scale, as well as its contribution to the formation of secondary organic aerosols.

Methods

Quantum chemical calculations

Quantum chemical calculations were performed using the Gaussian 09[29] and 16[31] software package. All the conformers were optimized using *ab initio* calculations at MP2 (Møller–Plesset second order perturbation theory) level of the theory[32]

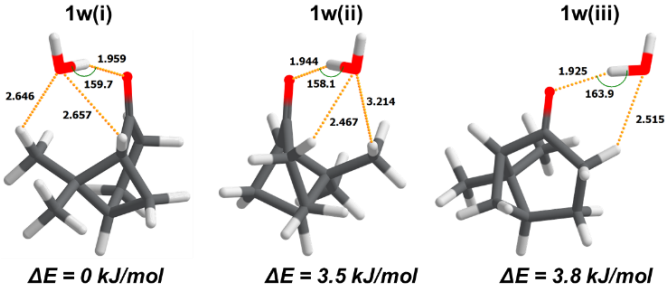

Figure 2. Optimized geometries at MP2/6-311++G(d,p) of observed three lowest energy conformers of NOP···H_2O. Bond length OH in (Å) and angle HOH in (°).

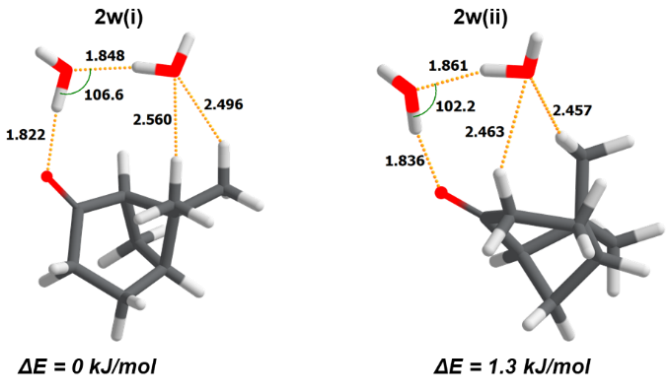

Figure 3. Optimized geometries at MP2/6-311++G(d,p) of the observed lowest energy conformers of NOP···$(H_2O)_2$. Bond length OH in (Å) and angle HOH in (°).

and ωB97X-D,[33,34] DFT, with the Pople split-valence triple-zeta basis set augmented with diffuse and polarization functions on all atoms (the 6-311++G(d,p) basis set). Also the two DFT methods B3LYP[35,36] including Grimme's dispersion correction (D3),[37] and the M06-2X[38,39] were used to optimize the structure of the possible structure of NOP-water complexes with the 6-311++G(2df,p) basis set.

The equilibrium rotational constants (*A, B, C*) and the quartic centrifugal distortion parameters (D_J, D_{JK}, D_K, d_1, d_2) as well as the electric dipole moment components have been calculated for the lowest energy conformers. Their values are presented in Tables 1-3 and compared to the obtained experimental parameters. All calculated conformers were optimized and confirmed to be true minima without negative harmonic vibrational frequencies. Three monohydrates were optimized by MP2 and M06-2X methods, see Figures 1 and 2. Surprisingly, only two monohydrates were optimized using B3LYP-D3 and ωB97X-D methods, the conformer 1w(ii) was not found because it converges to conformer 1w(iii). Six dihydrates and six trihydrates were optimized by the theoretical methods (MP2, M06-2X, B3LYP-D3 and ωB97X-D). Only the observed conformers are presented in Figure 2, Figure 3 and Figure 4. The molecular parameters of the non-observed dihydrates and trihydrates conformers of NOP···water are reported in the Supplementary Information.

An analysis of the relevant NBOs involved in the inter-molecular charge transfer responsible of the relative stability of the lowest energy conformer of nopinone···water, 1w(i) 2w(i) and 3w(i), was also performed[40] using M06-2X/6-311++G(2df,p). The same method was used to plot the map of the noncovalent

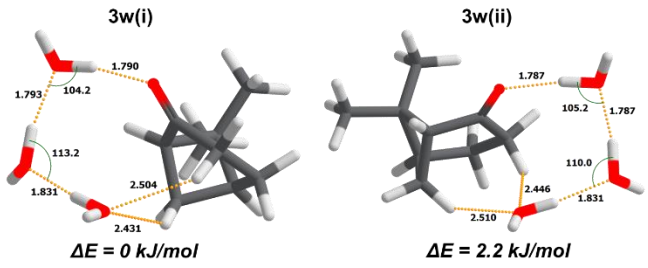

Figure 4. Optimized geometries at MP2/6-311++G(d,p) of the observed lowest energy conformers of NOP···$(H_2O)_3$ .The water chain in the two conformers have a quasi-mirror structure. Bond length OH in (Å) and angle HOH in (°).

interactions (NCI)[41] involved in the stabilisation of the observed conformers. This analysis was carried out using the Multiwfn software.[42] Further structure optimization using the MN15-L/6-311++G(d,p)[43] was performed, to better describe the structure of the 1w(ii) conformer. This method provides better description for non-covalent interaction and allow a better description of the rotational constants of conformer 1w(ii).

Experimental

The jet-cooled pure rotational (2–18 GHz) spectra of NOP-water complexes were recorded (see Figure 5) using Lille FP-FTMW spectrometer[44,45] coupled to supersonic jet. Nopinone (98%) was purchased as liquid samples from Sigma-Aldrich and was used without any further purification. The supersonic expansion was generated by expansion of neon (Ne) at stagnation pressure of 4 bar. Nopinone was placed in a nozzle and heated at about 343 K. Water was inserted in the gas line just before the nozzle. Then the mixture was introduced into the Fabry–Pérot cavity along the optical axis, through a 1 mm diameter pinhole of a pulsed nozzle at a repetition rate of 1.5 Hz. The rotational temperature (T_{Rot}) of the supersonic jet is estimated to be about a few Kelvin. Microwave power pulses of 2 µs duration were used to polarize the molecules. The Free Induction Decay (FID) signal was recorded using heterodyne detection at 30 MHz and digitized at a repetition rate of 120 MHz. FID signals were accumulated between 50 and 1000 times, depending on the line intensity to obtain a good signal-to-noise ratio. After a fast Fourier transformation of the time domain signals, lines were observed as Doppler doublets (≈10 kHz full width at half maximum, FWHM) due to the coaxial arrangement of the jet and the Fabry-Pérot cavity. Each resonance frequency was measured as the average frequency of the two Doppler components. The spectral resolution is depending on the number of recorded points. The frequency grid was set to 1.84 kHz, which was found sufficient since the Doppler width of the lines should be of several kHz.

Results and discussion

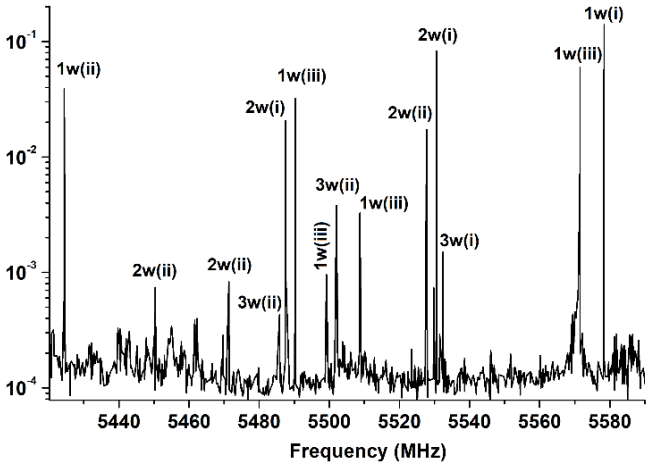

Figure 5. A portion of the experimental spectrum showing rotational lines of all the NOP-water clusters. The low-resolution scan mode of the FP-FTMW spectrometer was used. Intensity is in arbitrary units.

The main characteristic of rotational spectroscopy is the capability to provide accurate spectroscopic rotational parameters and when compared with those obtained by theoretical calculation leads to an unambiguous identification of the observed conformers. Theoretical calculations are used to help the analysis of the rotational spectra. According to those calculations, all the predicted conformers of NOP-water are asymmetric rotors and exhibit at least of one non-zero dipole moment component. The rotational spectra of all conformers were investigated by considering the output of MP2/6-311++G(d,p) level of theory and M06-2X/6-311++G(2df,p) since they predict an additional monohydrate. A wide scan has been performed to detect the possible conformers surviving in the adiabatic supersonic expansion. As shown in Figure 5, strong lines were assigned to complexes containing one water molecule; less intense lines were observed for cluster containing two water molecules and finally the weakest two spectra were assigned to the trihydrated conformers. For all observed conformers, transitions were measured experimentally at high-resolution and fitted to the experimental precision using Pickett's program[46] with a Watson's semi-rigid

Table 1. Experimental spectroscopic parameters for the three observed monohydrates of NOP compared with those predicted from *ab initio* MP2/6-311++G(d,p) and DFT M06-2X/6-311++G(2df,p) calculations.

	1w(i)		1w(ii)		1w(iii)	
Parameters [a]	**Exp.**	**Calc.** [e]	**Exp.**	**Calc.** [e]	**Exp.**	**Calc.** [e]
A	1322.42948(26)	1328|1335	1442.1291(18)	1637|1578	1748.772(10)	1758|1792
B	1005.490818(68)	1038|1076	768.49995(19)	769|836	705.91270(13)	708|716
C	756.541470(46)	774|797	719.00172(15)	720|772	669.09363(11)	671|681
D_J	0.30252(48)	0.23643|0.2093	1.93749(56)	3.7413|0.2091	0.76314(25)	0.6470|2.55
D_{JK}	-0.0376(24)	-0.1709|-0.1954	0.0808(30)	-18.09|-0.5855	-3.0402(37)	-2.135|-8.621
D_K	-0.166(16)	-0.025|0.059	-	26.1|0.893	-	8.287|34.40
d_1	-0.08892(24)	-0.0424|0.0587	-0.67501(73)	-0.5419|-0.033	-0.05412(35)	0.0587|-0.220
d_2	-0.00518(20)	0.01941|0.0188	-0.07650(43)	0.00956|-0.00005	0.00670(20)	-1.115|0.030
N [b]	82[f]	-	59[f]	-	48[g]	-
σ [c]	1.2	-	2.0	-	1.3	-
ΔE [d]	-	0	-	3.5	-	3.8

[a] *A, B, C* are the rotational constants given in MHz; D_J, D_{JK}, D_K, d_1 and d_2 are the quartic centrifugal distortion given in kHz; [b] Number of fitted transitions; [c] rms deviation of the fit in kHz; [d] ΔE represents the relative electronic energies in kJ mol^{-1} with respect to the global minima calculated at MP2/6-311++G(d,p); [e] calculated parameters at MP2/6-311++G(d,p) | M06-2X/6-311++G(2df,p); [f] a- and b-type transitions; [g] a-type transitions.

Table 2. Experimental spectroscopic parameters for the two observed dihydrates of NOP compared with those predicted from *ab initio* MP2/6-311++G(d,p) calculations.

	2w(i)		2w(ii)	
Para. [a]	**Exp.**	**Calc.** [e]	**Exp.**	**Calc.** [e]
A	1086.12505(96)	1098|1099	1263.5956(30)	1277|1267
B	685.249819(87)	690|719	561.264028(53)	569|599
C	520.101739(56)	524|546	529.294393(43)	541| 564
D_J	0.06498(41)	-|0.0681	0.13759(10)	-|0.14010
D_{JK}	0.7815(32)	-|0.4653	-0.1264(34)	-|-0.2844
D_K	-0.733(43)	-|-0.445	-	-|0.6929
d_1	-0.01398(19)	-|-0.0102	-0.00840(11)	-|-0.00557
d_2	-0.01222(19)	-|-0.0101	-	-|-0.00016
N [b]	74 [f]		39 [f]	
σ [c]	1.8		0.6	
ΔE [d]		0		1.3

[a] A, B and C are the rotational constants given in MHz; D_J, D_{JK}, D_K, d_1 and d_2 are the quartic centrifugal distortion given in kHz; [b] Number of fitted transitions; [c] rms deviation of the fit in kHz; [d] ΔE represents the relative electronic energies in kJ mol^{-1} with respect to the global minima calculated at MP2/6-311++G(d,p); [e] calculated parameters at MP2/6-311++G(d,p) | M06-2X/6-311++G(2df,p) level of theory; [f] a-type transitions.

rotor Hamiltonian[47] in the I^r representation and in the S-reduction.

As shown in Table 1, three different sets of experimental parameters have been assigned to the monohydrates, a total of 82, 59 and 48 transitions have been measured at high resolution. The calculated parameters predicted by MP2/6-311++G(d,p) and M06-2X/6-311++G(2df,p) calculations, are in good agreement with the experimental results.

For the dihydrates 74 and 39 lines have been fitted together to the two dihydrated conformers of NOP-$(H_2O)_2$. In the same way, two sets of rotational constants have been identified for the trihydrates by measuring 60 and 66 transitions for those species. The results are shown in Tables 2 and 3.

Table 3. Experimental spectroscopic parameters for the two observed trihydrates of NOP compared with those predicted from *ab initio* MP2/6-311++G(d,p) and DFT M06-X/6-311++G(2df,p) calculations.

	3w(i)		3w(ii)	
Para. [a]	**Exp.**	**Calc.** [e]	**Exp.**	**Calc.** [e]
A	872.0385(11)	885|892	1106.17164(22)	1147|1149
B	501.860939(57)	504|537	410.527409(34)	414|448
C	446.355960(53)	451|482	359.971675(23)	370|404
D_J	0.14100(12)	-|0.09372	0.098855(53)	-|0.0420
D_{JK}	-0.0541(14)	-|-0.1123	0.1371(11)	-|-0.05491
D_K	-	-|0.1479	0.756(19)	-|0.2805
d_1	-0.01360(13)	-|-0.01880	-0.000192(55)	-|-0.00616
d_2	-0.002691(95)	-|-0.0020	-0.000524(28)	-|-0.00033
N [b]	60[f]		66[g]	
σ [c]	0.8		0.6	
ΔE [d]	-	0	-	1.3

[a] A, B and C are the rotational constants given in MHz; D_J, D_{JK}, D_K, d_1 and d_2 are the quartic centrifugal distortion given in kHz; [b] Number of fitted transitions; [c] rms deviation of the fit in kHz; [d] ΔE represents the relative electronic energies in kJ mol^{-1} with respect to the global minima calculated at MP2/6-311++G(d,p). [e] calculated parameters at MP2/6-311++G(d,p)|M062-2X/6-311++G(2df,p); [f] a-type transitions. [g] a-type and c-type transitions.

The confirmation of the identity of the observed conformers can be done by comparing the calculated rotational constants to those observed experimentally. Moreover, for the observed clusters, the calculated dipole moments should be in good agreement with observed transition types, which led to an unambiguous identification of the observed clusters.

For the monohydrates it is evident that all the predicted conformers by MP2 and M06-2X have been observed. The calculated dipole moments are in good agreements with those predicted by MP2/6-311++G(d,p) (see SI). Unfortunately, despite the good parameters predicted by B3LYP-D3 and ωB97X-D for the 1w(i) and 1w(iii) (see SI), these two methods fail to predict the conformer 1w(ii) which exhibits an intense rotational spectrum. The complete comparisons of the experimental parameter to all the theoretical calculations are provided in the SI in the tables S1-S7.

In all the monohydrates, water is attached to NOP by a strong H-bonding interaction (O_w—H_w···O_{NOP}) and a weaker dispersive interaction between O_w and H_{NOP} (see Fig. 2). Interestingly, a good agreement between experimental results and MP2 calculations for 1w(i) and 1w(iii) but for the 1w(ii) conformer the error on the *A* rotational constant is quite high. The problem of such a discrepancy between experiment and theoretical calculation may become from the incomplete description of the non-covalent interactions between water oxygen and NOP hydrogen involved in the stabilization of the conformer 1w(ii). It has been reported that this MN15-L method[43] predicts better the weak non-covalent interaction. To test if any structural enhancement could be obtained using this method, we performed additional calculation using the MN15-L/6-311++G(d,p). Surprisingly, the calculated parameters by MN15-L/6-311++G(d,p) are in good agreement with those obtained experimentally. The discrepancy between the experimental (1442.2 MHz) and theoretical value at MN15-L (1534 MHz) of the *A* constant decreases significantly. The obtained rotational constants are compared to the experimental values in the supporting information (Table S8).

Another approach could be used by modifying the *ab initio* structure of 1w(ii) to better match the observed experimental constants. Since the rotational constants depend directly on the mass distribution of the atoms around the rotational axis (*a,b,c*). In order to decrease the error on the *A* constant, the position of the water molecule was modified by scanning both the dihedral angle O-O-C-C from 35.9° to 67.7° and the angle O-O-C from 104.4° to 119° for the conformer 1w(ii). With this scan, the error on the *A* constant was reduced remarkably which allows to better describe the observed structure of 1w(ii) monohydrate. In the modified structure, water molecule was found to be closer to the methyl group. This position allows the water molecule to take advantage of the stronger dispersive interaction offered by the methyl group. The modified structure is presented in the supporting information (Table S8).

For the dihydrated clusters, six different structures have been calculated by all the used theoretical methods. The identification of the lowest energy conformer 2w(i) is directly confirmed thanks to the good agreement between the observed and calculated rotational constants. The second set of

the observed rotational constants matches both conformers 2w(ii) and 2w(iii) (see SI), but their dipole moment components are different. Therefore, the assignment of the experimental data to the conformer 2w(ii) is straightforward due to the non-observation of any c-type transitions that should be observed for the conformer 2w(iii).

As for the monohydrated cluster, each dihydrate has the first water molecule forming a strong H-bonding with the NOP oxygen (O_w—H_w···O_{NOP}). Likewise, the oxygen of the second water for all dihydrates is stabilized in the mid-position between two hydrogens of NOP molecules by a bifurcated dispersive-bond. The structure of the two observed conformers is shown in Figure 3.

Concerning the trihydrated clusters, among the six calculated species (see the SI), only the two lowest energy conformers have been detected (see Figure 4), they have the smallest experimental signals. The structures of the trihydrated complex are stabilized by similar intermolecular interactions: a strong H-bond between the first water molecule and NOP (O_w—H_w···O_{NOP}) and finishing with a dispersive interaction H_w—O_w···H_{NOP}, analogously to the other hydrates.

The oxidation of β-pinene to NOP does not affect the bicycle structure.[28] Although NOP affects the structure of the pure water dimer and trimer. Indeed, intermolecular forces act in those clusters (H-bonding and dispersive interactions) and led to their deformation. For the dihydrates, the hydrogen between the two water molecules in 2w(i) and 2w(ii) complexes is shortened by 0.1 Å compared to the water dimer and the dihedral angle (∠H_{w2}-O_{w2}-H_{w2}-O_{w1}) value changes to 150.5° and -159.1° for both 2w(i) and 2w(ii), respectively, instead of 180° for the pure water dimer. For the trihydrate, the structure of those complexed to NOP is a chain and not a cycle but preserving a quasi-cyclic structure opening by around (∠O_{w1}-O_{w2}-O_{w3}) 40° more than in the pure water trimer. The arrangement of the water molecules in those clusters is characterized by a remarkable decreasing in the H-bonding length. We can also observe that H-bond length decreases when the number of water molecule increases. However, the presence of three water molecules promotes the cooperativity between H-bonds of the water molecules over stabilizing the species. As the three water molecules are not forming a close cycle, the H-bond interaction (O_w—H_w···O_{NOP}) together with the dispersive one break that cycle and oblige the water molecules to adapt their structure on NOP.

The stability of the lowest energy clusters of NOP···water, 1w(i), 2w(i) and 3w(i), can be traced back to a large extent to the strong inter-molecular interactions achieved in those complexes. Natural bond orbital (NBO) analysis provides an intuitive framework to rationalize the transfer of electronic charge associated with this interaction.[40] The NBO analysis were performed at M06-2X/6-311++G(2df,p) method for the lowest energy conformers NOP-water complexes (1w(i), 2w(i) and 3w(i)). The most relevant electronic transfers are shown in Figures 6, 7 and 8. The first general conclusion of the NBO analysis is that the intermolecular interactions can be explained in terms of 99% of Lewis structure and 1% of non-Lewis structure. These values reflect an appreciable degree of charge delocalization in the intermolecular H-bonds that stabilize the structure by one dominant interaction: the intermolecular interactions between lone pair of NOP oxygen and anti-bonding orbitals of O-H of water molecules. Concerning the 1w(i) conformer, the dominant interaction occurs between n orbital of O_{NOP} and BD* orbital of O_{w1}-H_{w1} with a stabilization energy of 21 kJ/mol. 2w(i) complex, shows similar charge transfers involving *n* orbital of O_{NOP} and BD* orbital of O_{w1}-H_{w1} with a stabilization energy of 15 and 43 kJ/mol. Moreover, new stabilization pathways involve the second H_2O molecule between lone pair orbital of O_{w1} (H_2O bonded to C=O of NOP) and BD* orbital of O_{w2}-H_{w2} (second H_2O) with a stabilization energy of 51 kJ/mol. Finally, the 3w(i) complex shows similar features to mono- and dihydrate complexes with similar stabilization energies. Additionally, the third water molecule plays also an important role in the stabilization of the complex

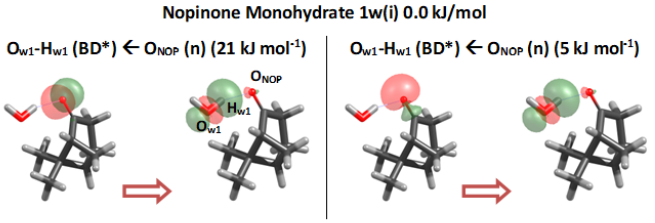

Figure 6. Most relevant NBOs involved in the inter-molecular charge transfer responsible of the relative stability of the lowest energy monohydrate 1w(i) calculated at the M06-2X/6-311++G(2df,p) level of theory.

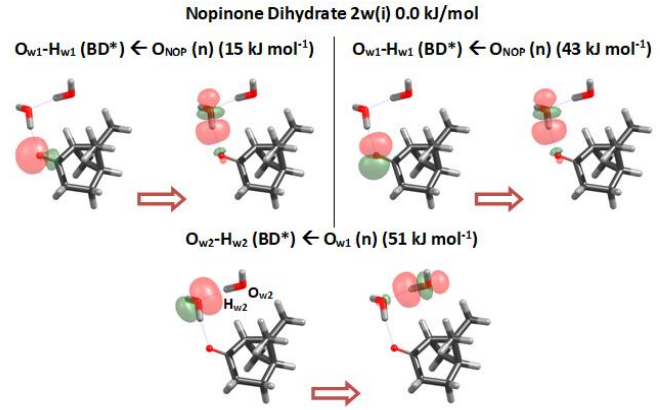

Figure 7. Most relevant NBOs involved in the inter-molecular charge transfer responsible of the relative stability of the lowest energy dihydrate 2w(i) calculated at the M06-2X/6-311++G(2df,p) level of theory.

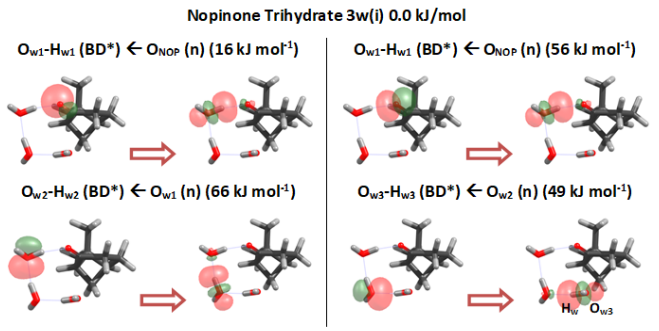

Figure 8. Most relevant NBOs involved in the inter-molecular charge transfer responsible of the relative stability of the lowest energy trihydrate 3w(i) calculated at the M06-2X/6-311++G(2df,p) level of theory.

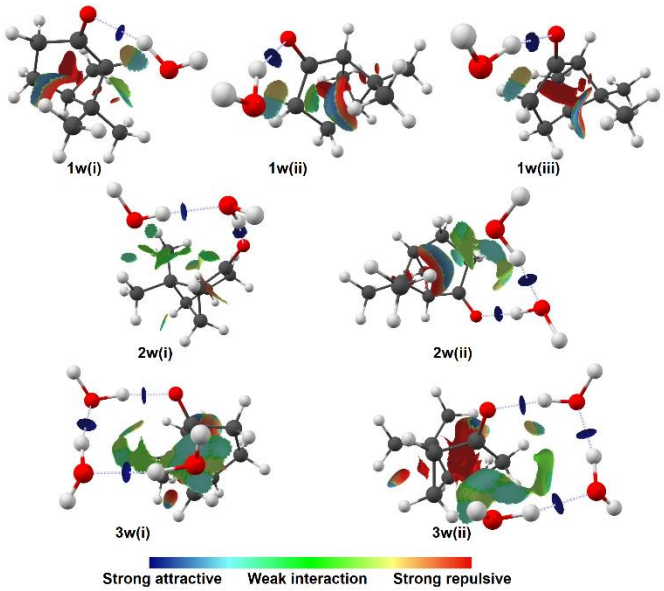

Figure 9. NCI plots showing the most relevant interactions responsible of the relative stability of the observed conformers of NOP···$(H_2O)_n$ (n=1,2,3).

by a charge transfer between lone pair orbital of O_{w2} (second H_2O) and BD* orbital of O_{w3}-H_{w3} (third H_2O) with a stabilization energy of 49 kJ/mol.

Another interesting analysis was performed using Non-Covalent Interactions (NCI) method[41] in order to visualize the interactions involved in the stabilization of the observed species of NOP···water complexes. The NCI analysis is in good agreement with the NBO analysis and confirms the existence of a strong hydrogen bond and two additional weak hydrogen bonds interaction between water and NOP. As shown in the Figure 9 the dark blue iso-surface indicate strong hydrogen bonds. The weak attractive interactions are shown in the green iso-surface. These interactions play an important key role in the stabilization and the preference of the observed conformer of NOP···water complexes. As can be observed in the Figure 9., for the trihydrates 3w(i) and 3w(ii) the map of the dispersive interaction is very important and involve both O_{w2} and O_{w3} participating directly to their stabilization. To plot the map of the interactions involved in the stabilisation of the observed conformer, noncovalent interaction (NCI) analysis was carried out using the Multiwfn software[42] from the M06-2X/6-311++G(2df,p) level output.

Regarding similar hydrated bicyclic ketones in the literature, such as camphor[19] and verbenone[26], NOP[28] has a similar bicyclic structure to verbenone, the only difference that in the case of verbenone the carbon C_4 is attached to a methyl group and an endocyclic double bond links C_3=C_4. The bicyclic unite of camphor (Bicyclo[2.2.1]heptane) molecule is different than that of NOP (Bicyclo[3.1.1]heptane). In both cases NOP has one carbon less than verbenone and camphor. For both camphor and verbenone, two dihydrated conformers have been observed, but only two monohydrated and one trihydrated conformers have been reported.[19,26] In the present study, the unique structure of NOP, that its structure is slightly different to verbenone and camphor, we observed further one monohydrate and one trihydrate. This could be explained by the dispersive interactions offered by the NOP molecule which enhanced the stabilization of further one monohydrate and one trihydrate clusters. Therefore, this study highlights how the structural changes in the NOP compared to camphor and verbenone molecules leads to a richer conformational landscape in the case of NOP···water. By comparing the water chain structure in the observed trihydrates of our study to that observed in the case of camphor and verbenone we can observe that $\angle O_{w1}$-O_{w2}-O_{w3} of water molecules are closer to the trihydrate of camphor than the verbenone. For 3w(i) and 3w(ii), the calculated values at MP2/6-311++G(d,p) level of theory of $\angle O_{w1}$-O_{w2}-O_{w3} are 105.1° and 100.8°, respectively. Their values ($\angle O_{w1}$-O_{w2}-O_{w3}) at the same method MP2/6-311++G(d,p) in the case of verbenone and camphor are 122.4° and 102.2°, respectively. This observation is very important and explains how the water chain adapts its structure to the ketone molecule. In the same way, the dihydrates of NOP adapt similar structure to those observed in the case of camphor and verbenone in which the water dimer adjusts its structure on the host molecule.

The favourite hydration sites obtained in this study could also be compared to the favourite hydrogen atom abstraction obtained from a computational study[48] using high-level calculations in order to simulate the atmospheric oxidation of NOP with OH radical. Surprisingly, these hydrogen atom abstractions match with the favourite hydration sites found in our study and where the dispersive interactions stabilize the oxygen of the water molecule of the observed conformers.

Conclusions

In summary, the synergic combination of FP-FTMW spectrometer with theoretical calculations have led to the identification of the hydrated NOP structure up to three water molecules. The optimisation of monohydrate conformers with the B3LYP-D3 and ωB97X-D methods missed one monohydrate, while the MP2 and M06-2X methods reproduce qualitatively all the three observed monohydrates. For the 1w(ii) conformer the structure of water molecule obtained at MP2/6-311++G(d,p) was modified in order to better reproduce the experimental data. For the dihydrates and trihydrates the observed experimental structures have been perfectly predicted with all the theoretical methods performed in this study. The observed structures of the di- and trihydrate complexes are stabilized by strong inter-molecular interactions. The formation of the hydrogen bond with the NOP molecule alters the structure of the water dimer and trimer. The formation of hydrogen bond was also discussed by performing NBO and NCI analysis. In addition, this study emphasizes the importance of the molecular structure which gives rise to additional dispersive interactions and increase the number of the observed hydrates. These results could be useful as starting point to study atmospheric oxidation of BVOC's toward understanding the mechanism of the aerosol formation starting from the formation of H-bonding.

Conflicts of interest

There are no conflicts to declare

Acknowledgements

The present work was funded by the French ANR Labex CaPPA through the PIA under contract ANR-11-LABX-0005-01, by the Regional Council Hauts-de-France and by the European Funds for Regional Economic Development (FEDER). It is a contribution to the scientific project CPER CLIMIBIO. E.M.N. would like to thank Dr. V. Vallet and Dr. F. Réal for the remote use of the PhLAM Linux clusters to perform the calculations.

Notes and references

1 J. Lelieveld, T. M. Butler, J. N. Crowley, T. J. Dillon, H. Fischer, L. Ganzeveld, H. Harder, M. G. Lawrence, M. Martinez, D. Taraborrelli and J. Williams, *Nature*, 2008, **452**, 737–740.

2 M. Hallquist, J. C. Wenger, U. Baltensperger, Y. Rudich, D. Simpson, M. Claeys, J. Dommen, N. M. Donahue, C. George, A. H. Goldstein, J. F. Hamilton, H. Herrmann, T. Hoffmann, Y. Iinuma, M. Jang, M. E. Jenkin, J. L. Jimenez, A. Kiendler-Scharr, W. Maenhaut, G. McFiggans, T. F. Mentel, A. Monod, A. S. H. Prévôt, J. H. Seinfeld, J. D. Surratt, R. Szmigielski and J. Wildt, *Atmos. Chem. Phys.*, 2009, **9**, 5155–5236.

3 R. Zhang, *Science*, 2010, 328, 1366–1367.

4 M. Kanakidou, J. H. Seinfeld, S. N. Pandis, I. Barnes, F. J. Dentener, M. C. Facchini, R. Van Dingenen, B. Ervens, A. Nenes, C. J. Nielsen, E. Swietlicki, J. P. Putaud, Y. Balkanski, S. Fuzzi, J. Horth, G. K. Moortgat, R. Winterhalter, C. E. L. Myhre, K. Tsigaridis, E. Vignati, E. G. Stephanou and J. Wilson, *Organic aerosol and global climate modelling: a review*, 2005, vol. 5.

5 A. C. Vander Wall, V. Perraud, L. M. Wingen and B. J. Finlayson-Pitts, *Environ. Sci. Process. Impacts*, 2020, **22**, 66–83.

6 M. Kulmala, L. Pirjola and J. M. Mäkelä, *Nature*, 2000, **404**, 66–69.

7 Q. Zhang and L. Du, *Comput. Theor. Chem.*, 2016, **1078**, 123–128.

8 D. R. Cocker, S. L. Clegg, R. C. Flagan and J. H. Seinfeld, *Atmos. Environ.*, 2001, **35**, 6049–6072.

9 C. J. Hennigan, M. H. Bergin, J. E. Dibb and R. J. Weber, *Geophys. Res. Lett.*, 2008, **35**, L18801.

10 C. J. Hennigan, M. H. Bergin and R. J. Weber, *Environ. Sci. Technol.*, 2008, **42**, 9079–9085.

11 G. A. Jeffrey, *An Introduction to Hydrogen Bonding*, Oxford University Press, Oxford, 1997.

12 E. N. Baker and R. E. Hubbard, *Prog. Biophys. Mol. Biol.*, 1984, 44, 97–179.

13 E. M. Neeman and T. R. Huet, *Phys. Chem. Chem. Phys.*, 2018, **20**, 24708–24715.

14 E. M. Neeman and T. R. Huet, *Phys. Chem. Chem. Phys.*, 2021, **23**, 2179–2185.

15 J. R. A. Moreno, T. R. Huet and J. J. L. González, *Struct. Chem.*, 2013, **24**, 1163–1170.

16 J. Thomas, O. Sukhorukov, W. Jäger and Y. Xu, *Angew. Chemie Int. Ed.*, 2014, **53**, 1156–1159.

17 C. Pérez, J. L. Neill, M. T. Muckle, D. P. Zaleski, I. Peña, J. C. Lopez, J. L. Alonso and B. H. Pate, *Angew. Chemie*, 2015, **127**, 993–996.

18 O. Bin, T. G. Starkey and B. J. Howard, *J. Phys. Chem. A*, 2007, **111**, 6165–6175.

19 C. Pérez, A. Krin, A. L. Steber, J. C. López, Z. Kisiel and M. Schnell, *J. Phys. Chem. Lett.*, 2016, **7**, 154–160.

20 C. Pérez, A. L. Steber, A. M. Rijs, B. Temelso, G. C. Shields, J. C. Lopez, Z. Kisiel and M. Schnell, *Phys. Chem. Chem. Phys.*, 2017, **19**, 14214–14223.

21 C. Pérez, M. T. Muckle, D. P. Zaleski, N. A. Seifert, B. Temelso, G. C. Shields, Z. Kisiel and B. H. Pate, *Science*, 2012, **336**, 897–901.

22 J. R. Aviles-Moreno, J. Demaison and T. R. Huet, *J. Am. Chem. Soc.*, 2006, **128**, 10467–10473.

23 M. Fatima, D. Maué, C. Pérez, D. S. Tikhonov, D. Bernhard, A. Stamm, C. Medcraft, M. Gerhards and M. Schnell, *Phys. Chem. Chem. Phys.*, 2020, **22**, 27966–27978.

24 N. S. Venkataramanan, *J. Mol. Model.*, 2016, **22**, 1–11.

25 D. Kumar Deb and B. Sarkar, *Phys. Chem. Chem. Phys.*, 2017, **19**, 2466–2478.

26 M. Chrayteh, A. Savoia, T. R. Huet and P. Dréan, *Phys. Chem. Chem. Phys.*, 2020, **22**, 5855–5864.

27 R. Winterhalter, P. Neeb, D. Grossmann, A. Kolloff, O. Horie and G. Moortgat, *J. Atmos. Chem.*, 2000, **35**, 165–197.

28 E. M. Neeman, J. R. Avilés-Moreno and T. R. Huet, *Phys. Chem. Chem. Phys.*, 2017, **19**, 13819–13827.

29 M. J. Frisch, G. W. Trucks, H. B. Schlegel, G. E. Scuseria, M. A. Robb, J. R. Cheeseman, G. Scalmani, V. Barone, B. Mennucci, G. A. Petersson, H. Nakatsuji, M. Caricato, X. Li, H. P. Hratchian, A. F. Izmaylov, J. Bloino, G. Zheng, J. L. Sonnenberg, M. Hada, M. Ehara, K. Toyota, R. Fukuda, J. Hasegawa, M. Ishida, T. Nakajima, Y. Honda, O. Kitao, H. Nakai, T. Vreven, J. J. A. Montgomery, J. E. Peralta, F. Ogliaro, M. Bearpark, J. J. Heyd, E. Brothers, K. N. Kudin, V. N. Staroverov, T. Keith, R. Kobayashi, J. Normand, K. Raghavachari, A. Rendell, J. C. Burant, S. S. Iyengar, J. Tomasi, M. Cossi, N. Rega, J. M. Millam, M. Klene, J. E. Knox, J. B. Cross, V. Bakken, C. Adamo, J. Jaramillo, R. Gomperts, R. E. Stratmann, O. Yazyev, A. J. Austin, R. Cammi, C. Pomelli, J. W. Ochterski, R. L. Martin, K. Morokuma, V. G. Zakrzewski, G. A. Voth, P. Salvador, J. J. Dannenberg, S. Dapprich, A. D. Daniels, O. Farkas, J. B. Foresman, J. V. Ortiz, J. Cioslowski and D. J. Fox, *Gaussian 09, Rev. B. 01*, Gaussian Inc., Wallingford, CT, 2010.

30 M. J. Frisch, G. W. Trucks, H. B. Schlegel, G. E. Scuseria, M. A. Robb, J. R. Cheeseman, G. Scalmani, V. Barone, B. Mennucci, G. A. Petersson, H. Nakatsuji, M. Caricato, X. Li, H. P. Hratchian, A. F. Izmaylov, J. Bloino, G. Zheng, J. L. Sonnenberg, M. Hada, M. Ehara, K. Toyota, R. Fukuda, J. Hasegawa, M. Ishida, T. Nakajima, Y. Honda, O. Kitao, H. Nakai, T. Vreven, J. J. A. Montgomery, J. E. Peralta, F. Ogliaro, M. Bearpark, J. J. Heyd, E. Brothers, K. N. Kudin, V.

N. Staroverov, T. Keith, R. Kobayashi, J. Normand, K. Raghavachari, A. Rendell, J. C. Burant, S. S. Iyengar, J. Tomasi, M. Cossi, N. Rega, J. M. Millam, M. Klene, J. E. Knox, J. B. Cross, V. Bakken, C. Adamo, J. Jaramillo, R. Gomperts, R. E. Stratmann, O. Yazyev, A. J. Austin, R. Cammi, C. Pomelli, J. W. Ochterski, R. L. Martin, K. Morokuma, V. G. Zakrzewski, G. A. Voth, P. Salvador, J. J. Dannenberg, S. Dapprich, A. D. Daniels, O. Farkas, J. B. Foresman, J. V. Ortiz, J. Cioslowski and D. J. Fox, *Gaussian 09, Rev. E.01*, Gaussian Inc., Wallingford, CT, 2013.

31 M. J. Frisch, G. W. Trucks, H. B. Schlegel, G. E. Scuseria, M. A. Robb, J. R. Cheeseman, G. Scalmani, V. Barone, G. A. Petersson, H. Nakatsuji, X. Li, M. Caricato, A. V. Marenich, J. Bloino, B. G. Janesko, R. Gomperts, B. Mennucci, H. P. Hratchian, J. V. Ortiz, A. F. Izmaylov, J. L. Sonnenberg, D. Williams-Young, F. Ding, F. Lipparini, F. Egidi, J. Goings, B. Peng, A. Petrone, T. Henderson, D. Ranasinghe, V. G. Zakrzewski, J. Gao, N. Rega, G. Zheng, W. Liang, M. Hada, M. Ehara, K. Toyota, R. Fukuda, J. Hasegawa, M. Ishida, T. Nakajima, Y. Honda, O. Kitao, H. Nakai, T. Vreven, K. Throssell, J. A. Montgomery, Jr., J. E. Peralta, F. Ogliaro, M. J. Bearpark, J. J. Heyd, E. N. Brothers, K. N. Kudin, V. N. Staroverov, T. A. Keith, R. Kobayashi, J. Normand, K. Raghavachari, A. P. Rendell, J. C. Burant, S. S. Iyengar, J. Tomasi, M. Cossi, J. M. Millam, M. Klene, C. Adamo, R. Cammi, J. W. Ochterski, R. L. Martin, K. Morokuma, O. Farkas, J. B. Foresman and D. J. Fox, *Gaussian 16, Rev. C. 01*, 2016, Gaussian Inc., Wallingford, CT, 2019.

32 C. Møller and M. S. Plesset, *Phys. Rev.*, 1934, **46**, 618–622.

33 J. Da Chai and M. Head-Gordon, *J. Chem. Phys.*, 2008, **128**, 084106.

34 J. Da Chai and M. Head-Gordon, *Phys. Chem. Chem. Phys.*, 2008, **10**, 6615–6620.

35 A. D. Becke, *J. Chem. Phys.*, 1993, **98**, 5648–5652.

36 C. Lee, W. Yang and R. G. Parr, *Phys. Rev. B*, 1988, **37**, 785–789.

37 S. Grimme, *WIREs Comput. Mol. Sci.*, 2011, **1**, 211–228.

38 Y. Zhao and D. G. Truhlar, *Acc. Chem. Res.*, 2008, **41**, 157–167.

39 Y. Zhao and D. G. Truhlar, *Theor. Chem. Acc.*, 2008, **120**, 215–241.

40 J. P. Foster and F. Weinhold, *J. Am. Chem. Soc.*, 1980, **102**, 7211–7218.

41 E. R. Johnson, S. Keinan, P. Mori-Sánchez, J. Contreras-García, A. J. Cohen and W. Yang, *J. Am. Chem. Soc.*, 2010, **132**, 6498–6506.

42 T. Lu and F. Chen, *J. Comput. Chem.*, 2012, **33**, 580–592.

43 H. S. Yu, X. He and D. G. Truhlar, *J. Chem. Theory Comput.*, 2016, **12**, 1280–1293.

44 M. Tudorie, L. H. Coudert, T. R. Huet, D. Jegouso and G. Sedes, *J. Chem. Phys.*, 2011, **134**, 074314.

45 E. M. Neeman, J. R. Avilés Moreno and T. R. Huet, *J. Chem. Phys.*, 2017, **147**, 214305.

46 H. M. Pickett, *J. Mol. Spectrosc.*, 1991, **148**, 371–377.

47 J. K. G. Watson, in *Vibrational spectra and structure, vol.6. A series of advances*, 1977, pp. 1–89.

48 P. J. Lewis, K. A. Bennett and J. N. Harvey, *Phys. Chem. Chem. Phys.*, 2005, **7**, 1643–1649.